TELKOMNIKA Telecommunication, Computing, Electronics and Control
Vol. 24, No. 4, August 2026, pp. 1409∼1417
ISSN: 1693-6930, DOI: 10.12928/TELKOMNIKA.v24i4.27787

Extended-state observer control with online payload identification for HRI in series elastic actuators

Edwin Villarreal-López[1,2], Horacio Coral-Enriquez[2], Luini L. Hurtado-Cortés[3]
[1]Faculty of Engineering, Fundación Universitaria Los Libertadores, Bogotá, Colombia
[2]Faculty of Engineering, Universidad de San Buenaventura, Bogotá, Colombia
[3]Faculty of Engineering, Universidad Distrital Francisco José de Caldas, Bogotá, Colombia

Article Info

Article history:

Received Jan 8, 2026
Revised May 9, 2026
Accepted May 25, 2026

Keywords:

Active disturbance rejection control
Algebraic estimation
Human-robot interaction
Motion intention identification
Series elastic actuators

ABSTRACT

Safe human–robot interaction requires actuators that combine compliance with accurate force inference. Series elastic actuators (SEAs) are particularly suitable for this purpose; however, separating payload-induced torques from voluntary human interaction forces without dedicated sensors remains a critical challenge. This paper proposes a unified observer-based control framework for SEAs that integrates three key components: a linear parameter-varying extended state observer (LPV-ESO), an online algebraic payload estimator, and a disturbance-driven motion intention identification (MII) mechanism. The payload estimator continuously updates the observer gains to adapt to load variations, while the LPV-ESO decouples payload dynamics from human interaction forces. The disturbance estimate is then processed through the MII block to infer operator intent in real time without additional sensing hardware. Numerical simulations under nominal conditions and ±10% parametric uncertainty confirm bounded trajectory tracking error, rapid convergence of payload estimation, and effective separation of payload-induced torques from voluntary interaction forces. The results demonstrate that the proposed framework achieves sensorless force decomposition and reliable motion intention inference, offering a practical solution for SEA-based collaborative robots in rehabilitation, assistance, and industrial applications.

Corresponding Author:

Edwin Villarreal-López
Faculty of Engineering, Fundación Universitaria Los Libertadores
Bogotá, Colombia
Email: evillarreall@libertadores.edu.co

1. INTRODUCTION

The classical perspective of automation assigns robots to repetitive and hazardous tasks in structured industrial environments [1], [2]. However, the proliferation of robotic systems outside traditional manufacturing tasks has redefined the role of robots as collaborative agents operating in proximity to human workers [3]. In this context, human-robot interaction (HRI) systems are required to satisfy simultaneous demands for safety, adaptability, and performance [4].

HRI systems have been applied in rehabilitation and physical assistance, surgery [5], agriculture [6], customer service [7], and collaborative manufacturing [8]. Regardless of the application domain, three common requirements are identified in the literature: safety during physical contact, robustness to parametric uncertainty, and reliable detection of human motion intention.

Detection of human motion is commonly achieved by remote sensing such as laser rangefinders, infrared detectors, and depth cameras combined with tracking and gesture recognition algorithms [4]. An alternative is the use of contact sensors at the joints or end effectors, which provide direct measurements of applied forces and trajectory disturbances [9]. Machine learning methods applied to inertial measurement unit (IMU) and electromyography signals have demonstrated real-time motion intention detection performance suitable for exoskeleton control [10]. However, these sensor-based approaches introduce additional hardware, increase system cost and complexity, and require subject-specific calibration procedures.

Motion intention identification (MII) addresses the problem of detecting the desired movement of the operator [11]. Electromyography has been widely used for this purpose, but signal processing instability and long detection latency limit its applicability in robotic manipulators [12]. Reduced joint stiffness has been proposed as an alternative, although this approach requires displacement sensors and increases structural complexity. Admittance-based controllers and motor current feedback have also been explored for MII in collaborative manipulation [13]. These methods share a common limitation: they require additional sensors or impose restrictive assumptions on operating conditions, making sensorless MII under payload variation an open problem.

Series elastic actuators (SEA) offer inherent compliance, shock absorption, and indirect torque sensing from spring deflection without dedicated force sensors [14], [15], which has motivated their use in industrial manipulators, wearable orthoses, and rehabilitation devices [16]. Recent developments have addressed both their design and control: on the mechanical side, variable-stiffness mechanisms and tensile-spring array configurations have been proposed to improve compliance range and energy storage [17]; on the control side, active disturbance rejection control (ADRC) with an extended state observer (ESO) has been applied to SEA force and position regulation [18], with extensions to fractional-order formulations [19], ultra-local model structures, and dual-ESO schemes for flexible-joint robots [20]. Parameter identification frameworks for SEA have also been reported [21]. However, the integration of online payload estimation within the observer design, which is required to maintain prescribed control performance under disturbances, has not been addressed in the context of SEA-based HRI.

A further challenge is the online estimation of the payload mass when load variations occur during operation and additional sensors are to be avoided. Algebraic identification methods can compute parameter estimates in real time from joint angle measurements with convergence times suitable for adaptive control [22]. Disturbance observer and Kalman filter schemes with nonlinear friction compensation have also been applied to sensorless payload estimation in collaborative robots [23]. Despite these contributions, a unified framework that simultaneously identifies the payload online, adjusts observer parameters based on the estimated load, and distinguishes payload-induced disturbances from voluntary motion intention forces has not been reported.

This paper proposes a unified sensorless control and MII framework for SEAs robots subject to online payload variations. The main contributions are the integration of an online algebraic payload estimator into the observer design enabling continuous gain adaptation without force or torque sensors, a Luenberger ESO with payload-dependent gains capable of decoupling payload-induced dynamics from voluntary human interaction forces, and a sensorless MII approach based on the disturbance-filtered integration of the observer output to map the estimated interaction force into a desired joint trajectory.

The remainder of this paper is organized as: section 2 presents the dynamic model. Section 3 describes the proposed control scheme. Section 4 presents the simulation results, and conclusions are given in section 5.

2. SEA-DRIVEN PENDULUM

The SEA-driven pendulum includes a servo actuator connected to a rigid beam of mass m and length l through a rotational spring with stiffness k, and a payload mass m_l at the beam tip (Figure 1). The generalized coordinates are the actuator angle θ and the beam angle q, measured from vertical equilibrium.

Applying the Euler-Lagrange equations with viscous damping and a lumped disturbance ξ (encompassing Coulomb friction and human interaction forces) yields the equations of motion:

$$I_a\ddot{\theta} + \left(D_\theta + \frac{k_m^2}{R}\right)\dot{\theta} + k(\theta - q) = \frac{k_m k_h}{R}U \tag{1}$$

$$(J_b + m_l l^2)\ddot{q} + D_q\dot{q} + k(q-\theta) + (mgl_c + m_l gl)\cos(q) = \xi \tag{2}$$

where $J_b = I_b + ml_c^2$ is the payload-independent beam inertia, I_a is the actuator inertia, D_θ and D_q are viscous damping coefficients, l_c is the distance from the pivot to the beam centre of mass, and the back-electromotive force (EMF) term k_m^2/R has been absorbed into the actuator damping. The driving torque is $k_m k_h U/R$, where k_m, k_h, and R are the motor constant, power-circuit gain, and armature resistance, respectively. In (1) and (2) form a cascade structure coupled through the spring torque $k(\theta - q)$. Crucially, both the inertial and gravitational terms in (2) depend linearly on m_l, a property exploited by the algebraic estimator in section 3.

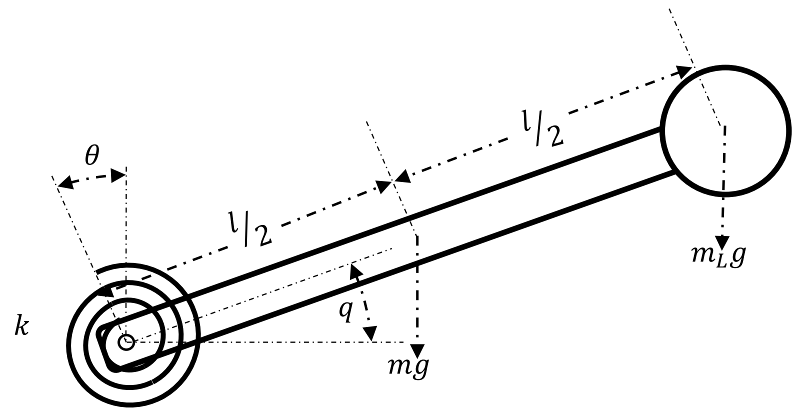

Figure 1. SEA-driven pendulum

3. HUMAN-ROBOT INTERACTION-BASED CONTROL SCHEME

From (2), the term ξ represents the lumped disturbance that includes the movement intention force and the uncertain dynamics and nonlinearities of the system. A sensorless approach for movement intention identification, robust to payload variations, is proposed. The control architecture consists of two loops: an inner loop that regulates the actuator angle θ, and an outer loop that governs the beam angle q under payload variations and movement intention forces. Figure 2 shows the proposed control scheme.

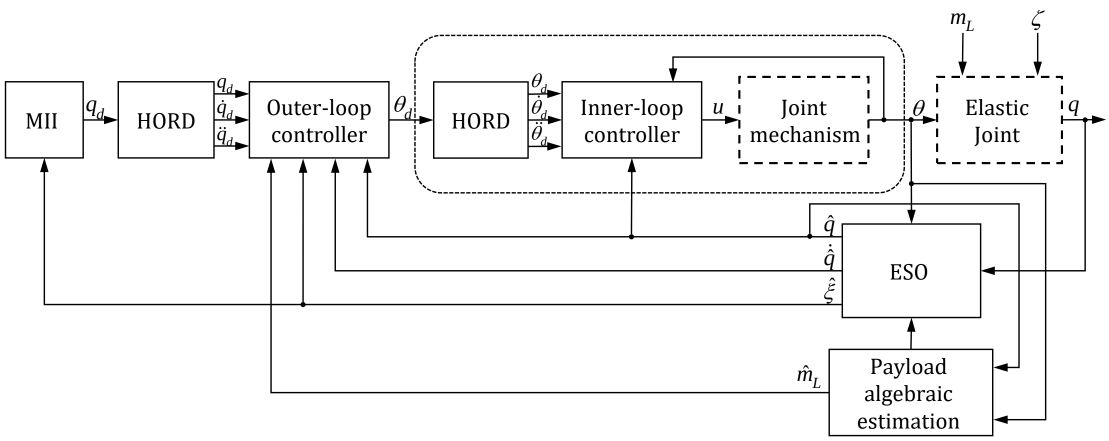

Figure 2. Proposed control scheme for the SEA mechanism for detection of movement intention

The outer loop provides estimates of the joint angle $\hat{q}$, velocity $\dot{\hat{q}}$, and lumped disturbance $\hat{\xi}$ through a parameter-varying ESO (LPV-ESO) whose gains are adjusted in real time based on the payload estimate $\hat{m}_l$ supplied by the algebraic identification block. The estimated disturbance $\hat{\xi}$ is used both for disturbance rejection in the control law and as the input signal to the MII block, which produces the desired joint angle q_d.

3.1. LPV ESO

An ESO based on the Luenberger structure is proposed for the outer loop. The observer parameters are adjusted in real time as a function of the estimated payload $\hat{m}_l$. From (2), the feedback linearization input is defined as:

$$\tau = k\theta - (mgl_c + gl\hat{m}_l)\cos(q) \tag{3}$$

which allows (2) to be rewritten as:

$$(J_b + l^2\hat{m}_l)\ddot{q} + D_q\dot{q} + kq - \tau = \xi \tag{4}$$

The extended state vector is defined as $x_1 = q$, $x_2 = \dot{q}$, and $x_3 = \xi$, where the disturbance is treated as a third state. Under the assumption of slowly varying disturbance, $\dot{\xi} \approx 0$, the following observer is proposed:

$$\begin{aligned} \dot{\hat{x}}_1 &= \hat{x}_2 + \lambda_3(x_1 - \hat{x}_1) \\ \dot{\hat{x}}_2 &= \frac{1}{J_b + l^2\hat{m}_l}(-k\hat{x}_1 - D_q\hat{x}_2 + \hat{x}_3 + \tau) + \lambda_2(x_1 - \hat{x}_1) \\ \dot{\hat{x}}_3 &= \lambda_1(x_1 - \hat{x}_1) \end{aligned} \tag{5}$$

Defining the estimation errors $e_i = x_i - \hat{x}_i$, the error dynamics reduce to the following third-order characteristic equation:

$$e_1^{(3)} + \left(\lambda_3 + \frac{D_q}{J_b + l^2\hat{m}_l}\right)\ddot{e}_1 + \left(\lambda_2 + \frac{\lambda_3 D_q + k}{J_b + l^2\hat{m}_l}\right)\dot{e}_1 + \frac{\lambda_1}{J_b + l^2\hat{m}_l}e_1 \approx 0 \tag{6}$$

The observer gains λ_i are selected by placing all three roots of (6) at $s = -\omega_o$, yielding the desired polynomial $(s + \omega_o)^3$. Matching coefficients gives:

$$\begin{aligned} \lambda_1 &= \omega_o^3\left(J_b + l^2\hat{m}_l\right) \\ \lambda_2 &= 3\omega_o^2 - \frac{\lambda_3 D_q + k}{J_b + l^2\hat{m}_l} \\ \lambda_3 &= 3\omega_o - \frac{D_q}{J_b + l^2\hat{m}_l} \end{aligned} \tag{7}$$

With this gain selection, all eigenvalues of the error dynamics are located at $s = -\omega_o$, guaranteeing exponential convergence of the estimation error in the absence of disturbance variations [24]. Under the condition that $\dot{\xi}$ is bounded, the estimation error remains ultimately bounded, with the steady-state bound inversely proportional to ω_o. It should be noted that the gains λ_i depend on $\hat{m}_l$ through the factor $J_b + l^2\hat{m}_l$ and are recalculated as the payload estimate is updated online, preserving the prescribed dynamics (6).

The selection of ω_o reflects a trade-off between estimation speed and robustness to measurement noise. Increasing ω_o accelerates convergence of e_1 to zero but also amplifies sensor noise in the disturbance estimate $\hat{x}_3$. Since $\hat{\xi}$ is used directly in the control law (13) and the MII block, excessive noise in $\hat{x}_3$ degrades trajectory tracking and trigger false intention activations. In this paper, $\omega_o = 4\omega_c$, where ω_c is the outer-loop bandwidth defined in section 4, provides a suitable compromise.

3.2. Online payload algebraic estimation

The payload mass $\hat{m}_l$ is identified online using the algebraic estimation approach ([25]). Applying the Laplace transform to (2) and treating ξ as a zero-mean rapidly varying noise term yields:

$$(J_b + m_l l^2)\left[s^2 q(s) - sq(0) - \dot{q}(0)\right] + D_q\left[sq(s) - q(0)\right] + kq(s) - k\theta(s) + (mgl_c + m_l gl)\chi(s) = 0 \tag{8}$$

where $\chi(s) = \mathcal{L}\{\cos(q(t))\}$. Taking consecutive derivatives with respect to s to eliminate the initial conditions, and multiplying by s^{-2} to avoid time differentiation and solving for $\hat{m}_l$:

$$\hat{m}_l = \frac{\alpha}{\beta} \tag{9}$$

where:

$$\alpha = \int^{(2)} \left[kt^2\theta - mgl_c\, t^2\chi - (2J_b + 2D_q t + kt^2)q\right] + \int (4J_b t + D_q t^2)q - J_b t^2 q \tag{10}$$

$$\beta = \int^{(2)} \left[2l^2 q + gl\, t^2\chi\right] - 4l^2 \int tq + l^2 t^2 q \tag{11}$$

Each of these expressions is implemented as a second-order time-varying filter. To attenuate the effect of the zero-mean noise ξ, a low-pass filter is included:

$$\begin{aligned}
&\alpha = z_1\\
&\dot{z}_1 = z_2 - J_b t^2 q\\
&\dot{z}_2 = z_3 + (4J_b t + D_q t^2)q\\
&\dot{z}_3 = kt^2\theta - mgl_c\, t^2\cos(q) - (2J_b + 2D_q t + kt^2)q\\
&\beta = z_4\\
&\dot{z}_4 = z_5 + l^2 t^2 q\\
&\dot{z}_5 = z_6 - 4l^2 tq\\
&\dot{z}_6 = 2l^2 q + gl\, t^2\cos(q)
\end{aligned} \tag{12}$$

The filters must be reset at the beginning of each estimation interval, and the estimate $\hat{m}_l$ is considered valid after a convergence period, as reported in section 4. It is important to note that the algebraic formulation assumes ξ to be a zero-mean noise term during the identification phase. In physical HRI scenarios, the operator may apply interaction forces simultaneously with the estimation procedure, introducing a non-zero mean component in ξ that biases the estimate $\hat{m}_l$. To mitigate this effect, the estimation is restricted to intervals in which $|\hat{\xi}|$ remains below the movement intention threshold γ (section 3.4.), which serves as a practical indicator of a no-interaction phase and allows the estimator to operate with reduced bias. This restriction is acknowledged as a limitation of the proposed approach in section 5.

3.3. Outer-loop control law

By means of feedback linearization applied to (2), and using the ESO estimates $\hat{q}$, $\dot{\hat{q}}$, and $\hat{\xi}$, the outer-loop control law establishes the actuator angle reference θ as:

$$\theta = \frac{1}{k}\left[D_q\dot{\hat{q}} + k\hat{q} + (mgl_c + gl\hat{m}_l)\cos(\hat{q}) - \hat{\xi}\right] + \frac{J_b + l^2\hat{m}_l}{k}\left[\ddot{q}_d - k_2(\dot{\hat{q}} - \dot{q}_d) - k_1(\hat{q} - q_d)\right] \tag{13}$$

where q_d is the desired joint angle. Substituting (13) into (2), the tracking error $e_t = q_d - q$ satisfies:

$$\ddot{e}_t + k_2\dot{e}_t + k_1 e_t \approx \varepsilon \tag{14}$$

where ε depends on the estimation errors and converges to zero as the observer errors decay. The controller gains are selected according to the desired bandwidth ω_c:

$$k_1 = \omega_c^2, \qquad k_2 = 2\omega_c \tag{15}$$

3.4. Movement intention identification

Figure 3 describes the movement intention identification scheme. The estimated disturbance $\hat{\xi}$ produced by the LPV-ESO contains both high-frequency components associated with fast actuator dynamics and low-frequency components correlated with the voluntary interaction force of the operator. A low-pass filter with cutoff frequency ω_f is applied to attenuate the high-frequency content:

$$\hat{\xi}_f(t) = \hat{\xi}(t)\frac{\omega_f}{s + \omega_f} \tag{16}$$

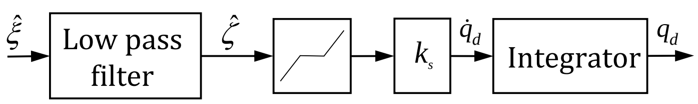

Figure 3. Proposed MII scheme

A deadband of threshold γ is then applied to $\hat{\xi}_f$ to suppress activations caused by residual noise and minor disturbances not associated with voluntary human intent. The remaining signal is scaled by a sensitivity gain k_s and integrated to produce the desired joint velocity $\dot{q}_d$:

$$\dot{q}_d(t) = \begin{cases} 0 & |\hat{\xi}_f(t)| < \gamma \\ k_s\hat{\xi}_f(t) & |\hat{\xi}_f(t)| \geq \gamma \end{cases} \tag{17}$$

The desired joint angle q_d is obtained by integration of $\dot{q}_d$.

The cutoff frequency ω_f determines the trade-off between sensitivity and response time: a lower value provides smoother estimates of the intention force but introduces a larger detection delay, while a higher value reduces delay at the cost of increased noise in $\hat{\xi}_f$. The value $\omega_f = 5$ rad/s is selected to achieve a response time compatible with typical human motion frequencies, which are generally below 2 Hz [11]. The deadband threshold γ is set to prevent activation by noise components that persist after low-pass filtering; its value is chosen above the observed noise floor of $\hat{\xi}_f$ under no-interaction conditions. The sensitivity gain k_s maps the magnitude of the filtered disturbance to the desired joint velocity: a larger value increases the range of motion per unit of applied force, while a smaller value requires greater operator effort.

4. RESULTS

Numerical simulations are performed to evaluate the proposed control scheme under nominal conditions and under $\pm 10\%$ random parameter variations. The mechanical parameters of the SEA-driven pendulum are: beam mass $m = 0.46$ kg, nominal load mass $m_l = 0.5$ kg, beam length $l = 0.2$ m, center-of-mass distance $l_c = 0.1$ m, beam inertia $I_b = 0.0015$ kg·m^2, actuator inertia $I_a = 0.001$ kg·m^2, actuator and beam damping $D_\theta = 0.05$ and $D_q = 0.02$ N·m·s/rad, and spring stiffness $k = 10$ N·m/rad. The motor parameters are $k_m = 0.05$ N·m/A, $R = 2.5\ \Omega$, and $k_h = 12$ V/PWM. The control parameters are set as follows: outer-loop bandwidth $\omega_c = 15$ rad/s, observer bandwidth $\omega_o = 4\omega_c = 60$ rad/s, MII filter cutoff $\omega_f = 5$ rad/s, sensitivity gain $k_s = 7$, and deadband threshold $\gamma = 0.1$ N·m. Two sets of results are presented: trajectory tracking under a predefined reference with small external disturbances, and payload estimation performance under online load variations.

4.1. Trajectory tracking

Trajectory tracking is evaluated in the absence of movement intention identification. A small external disturbance is applied at the end of the SEA-driven mechanism to emulate residual interaction forces. The payload is varied online each 10 seconds to examine the response of the system under load variations. Figure 4 presents the trajectory tracking results. Figure 4(a) shows the joint angle response over a 60-second simulation under nominal and under $\pm 10\%$ random parameter variations. The inset highlights the response around a payload transition, confirming that tracking error remains small in both scenarios. Figure 4(b) depicts the corresponding joint angle error. The tracking error stays bounded over the simulation under nominal and uncertain scenarios, as reported in Table 1. Peaks arise at payload variation instants and are attenuated by the outer loop, with settling times consistently below 2 s.

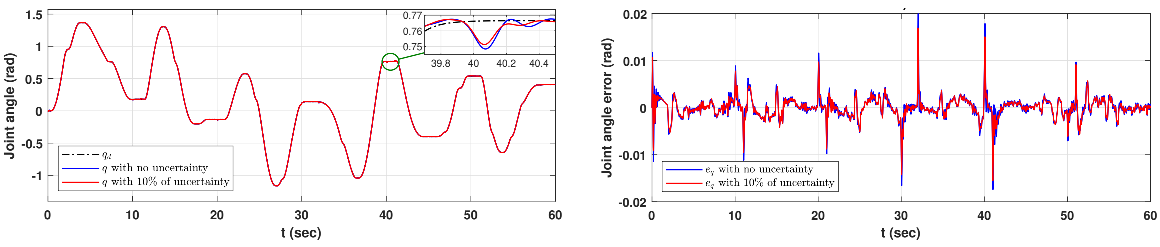

(a) (b)

Figure 4. Trajectory tracking results: (a) joint angle response under nominal and uncertain conditions and (b) joint angle tracking error

Table 1. Trajectory tracking performance metrics

Metric	Nominal	Uncertain (±10%)
Root mean square error (RMSE) — full simulation (rad)	0.0024	0.0022
RMSE — steady state (rad)	0.0022	0.0020
Mean absolute error (MAE) — steady state (rad)	0.0015	0.0014
Max error — full simulation (rad)	0.0199	0.0169
Peak error at $t = 20$ s (rad)	0.0116	0.0097
Settling time at $t = 20$ s (s)	1.42	1.87
Peak error at $t = 40$ s (rad)	0.0179	0.0155
Settling time at $t = 40$ s (s)	1.73	1.79

4.2. Payload estimation

Figure 5 shows the results of the online payload estimation. Figure 5(a) presents the real and estimated payload mass under nominal and uncertain conditions. After each variation, the algebraic estimator filters must be restarted and a convergence period of approximately two seconds is required before a valid estimate is available. During this interval, the load variation is treated as a lumped disturbance and rejected by the outer-loop control law, as reflected by the transient spikes observed in Figure 5(b).

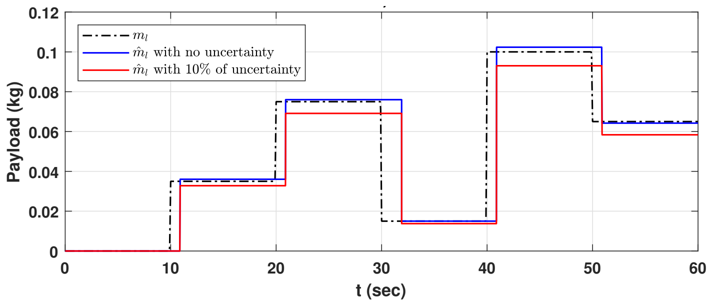

(a)

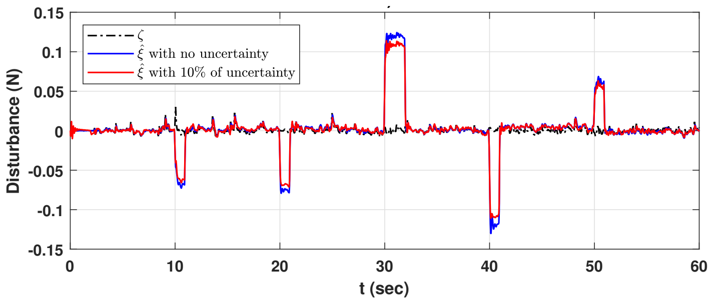

(b)

Figure 5. Payload estimation and disturbance results: (a) real and estimated payload mass under nominal and uncertain conditions and (b) real and estimated disturbance signals

Table 2 summarizes the payload estimation performance. Under both nominal and uncertain conditions the estimation error after convergence is small, consistent with the dependence of the algebraic estimator on the plant parameters. Once the payload estimate has converged and is incorporated into the observer gains (7), the disturbance estimate $\hat{\xi}$ returns to a low steady-state level, confirming that the LPV-ESO effectively separates payload-induced torques from residual disturbances. During each payload transition the peak disturbance is bounded and proportional to the magnitude of the load change, as shown in Figure 5(b).

Steady-state payload RMSE shown in Table 2 is affected by convergence transients, which produce large instantaneous errors immediately after load changes. Once convergence is achieved, the estimation error is significantly reduced, as reflected by the per-change values reported in the same table. The higher RMSE under nominal conditions, compared to the uncertain case, reflects the longer duration of the estimation transients.

The low steady-state level of $|\hat{\xi}|$ confirms that, once the payload estimate has converged, the lumped disturbance primarily reflects voluntary operator interaction forces rather than payload-induced torques. Preliminary simulations with deliberate interaction forces confirm that $\hat{\xi}_f$ exceeds the deadband threshold γ during intentional contact, activating the MII integrator and producing smooth trajectory adaptation consistent with the direction and magnitude of the applied force.

Table 2. Payload estimation and disturbance metrics

Metric	Nominal	Uncertain ($\pm 10\%$)
Estimation error at $t = 20$ s (kg)	0.0010	0.0059
Estimation error at $t = 40$ s (kg)	0.0024	0.0070
Payload RMSE — steady state (kg)	0.0133	0.0125
Peak $\|\hat{\xi}\|$ at $t = 20$ s (N·m)	0.0793	0.0714
Peak $\|\hat{\xi}\|$ at $t = 40$ s (N·m)	0.1302	0.1108
Disturbance RMSE — steady state (N·m)	0.0252	0.0229
Mean $\|\hat{\xi}\|$ — steady state (N·m)	0.0090	0.0084

5. CONCLUSION

A sensorless control scheme for SEA-driven robots that integrates online payload identification, parameter varying state estimation, and movement intention recognition has been proposed. The three components operate within a unified active disturbance rejection framework: the algebraic estimator provides the payload mass required to adjust the LPV-ESO gains, the observer supplies the disturbance estimate used both for control and for intention detection, and the MII block translates the filtered disturbance into a desired joint trajectory.

Simulation results under nominal conditions and under random parameter variations confirm that trajectory tracking error remains bounded throughout load transitions, with low steady-state RMSE in both cases. The algebraic estimator converges to the true payload value after each load change, with small relative estimation error under nominal conditions. The disturbance estimate returns to a low steady-state level after each convergence period, confirming that the observer gain adaptation effectively removes the payload contribution from the lumped disturbance signal. The structure of the observer output confirms that payload-induced torques and voluntary operator interaction forces produce distinguishable signatures in the estimated disturbance $\hat{\xi}$, consistent with the intended operating principle of the MII block.

FUNDING INFORMATION

This work was supported by the Fundación Universitaria Los Libertadores under the “Thirteenth Annual Internal Call for Research and Artistic and Cultural Creation Projects” [grant number: ING-10-24], as part of the doctoral research in Engineering of the first author at the Universidad Distrital Francisco José de Caldas.

AUTHOR CONTRIBUTIONS STATEMENT

This journal uses the Contributor Roles Taxonomy (CRediT) to recognize individual author contributions, reduce authorship disputes, and facilitate collaboration.

Name of Author	C	M	So	Va	Fo	I	R	D	O	E	Vi	Su	P	Fu
Edwin Villarreal-López	✓	✓	✓	✓	✓	✓		✓	✓	✓	✓	✓	✓	✓
Horacio Coral-Enriquez	✓	✓			✓				✓	✓		✓		
Luini L. Hurtado-Cortés		✓	✓	✓	✓				✓	✓				

C	: **C**onceptualization	I	: **I**nvestigation	Vi	: **Vi**sualization
M	: **M**ethodology	R	: **R**esources	Su	: **Su**pervision
So	: **So**ftware	D	: **D**ata Curation	P	: **P**roject Administration
Va	: **Va**lidation	O	: Writing - **O**riginal Draft	Fu	: **Fu**nding Acquisition
Fo	: **Fo**rmal Analysis	E	: Writing - Review & **E**diting		

CONFLICT OF INTEREST STATEMENT

The authors declare no conflict of interest.

DATA AVAILABILITY

The data that support the findings of this study are available from the corresponding author, Edwin Villarreal-López, upon reasonable request.

REFERENCES

[1] E. Dahlin, "Are robots stealing our jobs?" *Socius*, vol. 5, p. 2378023119846249, 2019, doi: 10.1177/2378023119846249.

[2] Z. M. Bi, C. Luo, Z. Miao, B. Zhang, W. J. Zhang, and L. Wang, "Safety assurance mechanisms of collaborative robotic systems in manufacturing," *Robotics and Computer-Integrated Manufacturing*, vol. 67, p. 102022, 2021, doi: 10.1016/j.rcim.2020.102022.

[3] M. M. Rahman, F. Khatun, I. Jahan, R. Devnath, and M. A.-A. Bhuiyan, "Cobotics: the evolving roles and prospects of next-generation collaborative robots in Industry 5.0," *Journal of Robotics*, vol. 2024, no. 1, p. 2918089, 2024, doi: 10.1155/2024/2918089.

[4] J. Arents, V. Abolins, J. Judvaitis, O. Vismanis, A. Oraby, and K. Ozols, "Human–robot collaboration trends and safety aspects: A systematic review," *Journal of Sensor and Actuator Networks*, vol. 10, no. 3, p. 48, 2021, doi: 10.3390/jsan10030048.

[5] E. Fosch-Villaronga, P. Khanna, H. Drukarch, and B. Custers, "The Role of Humans in Surgery Automation: Exploring the Influence of Automation on Human–Robot Interaction and Responsibility in Surgery Innovation," *International Journal of Social Robotics*, vol. 15, no. 3, pp. 563–580, 2023, doi: 10.1007/s12369-022-00875-0.

[6] L. Benos, V. Moysiadis, D. Kateris, A. C. Tagarakis, P. Busato, S. Pearson, and D. Bochtis, "Human-robot interaction in agriculture: a systematic review," *Sensors*, vol. 23, no. 15, p. 6776, 2023, doi: 10.3390/s23156776.

[7] N. Gasteiger, M. Hellou, and H. S. Ahn, "Factors for personalization and localization to optimize human-robot interaction: A literature review," *International Journal of Social Robotics*, vol. 15, no. 4, pp. 689–701, 2023, doi: 10.1007/s12369-021-00811-8.

[8] S. Hajzargarbashi, G. Côté, J. Boisvert, R. Meziane, C. Xu, C. Hubert, S. Jocelyn, and C. Gosselin, "Collaborative Robotic Finishing Platform for Metal Part Processing Towards Industry 5.0," *Advances in Transdisciplinary Engineering*, vol. 71, pp. 696 – 712, 2025, doi: 10.3233/ATDE250392.

[9] P. K. Murali, K. Darvish, and F. Mastrogiovanni, "Deployment and evaluation of a flexible human–robot collaboration model based on AND/OR graphs in a manufacturing environment," *Intelligent Service Robotics*, vol. 13, pp. 439–457, 2020, doi: 10.1007/s11370-020-00332-9.

[10] J.-J. Lin, C.-K. Hsu, W.-L. Hsu, T.-C. Tsao, F.-C. Wang, and J.-Y. Yen, "Machine Learning for Human Motion Intention Detection," *Sensors*, vol. 23, no. 16, 2023, doi: 10.3390/s23167203.

[11] D. Su, Z. Hu, J. Wu, P. Shang, and Z. Luo, "Review of adaptive control for stroke lower limb exoskeleton rehabilitation robot based on motion intention recognition," *Frontiers in Neurorobotics*, vol. 17, 2023, doi: 10.3389/fnbot.2023.1186175.

[12] F. Gao, L. Wang, and T. Lin, "Intelligent wearable rehabilitation robot control system based on mobile communication network," *Computer Communications*, vol. 153, pp. 286–293, 2020, doi: 10.1016/j.comcom.2020.01.054.

[13] C. Shen, M. Cheng, B. Sun, and B. Xu, "Hydraulic Dual-arm Manipulator Coordinated Motion Control for Human-robot Collaborative Heavy Load Handling;," *Jixie Gongcheng Xuebao/Journal of Mechanical Engineering*, vol. 61, no. 15, pp. 162 – 173, 2025, doi: 10.3901/JME.2025.15.162.

[14] B. Zhong, K. Guo, H. Yu, and M. Zhang, "Toward gait symmetry enhancement via a cable-driven exoskeleton powered by series elastic actuators," *IEEE robotics and automation letters*, vol. 7, no. 2, pp. 786–793, 2021, doi: 10.1109/LRA.2021.3130639.

[15] H. Zhong, P. Li, L. Gao, and X. Li, "Low-delay Admittance Control of Hydraulic Series Elastic Actuator for Safe Human-Robot Collaboration," *Procedia Manufacturing*, vol. 48, pp. 147–153, 2020, doi: 10.1016/j.promfg.2020.05.031.

[16] E. Martey, B. Opoku-Antwi, and F. K. A. Nyarko, "Hand exoskeletons in stroke recovery: A systematic review of trends and technologies," *Scientific African*, vol. 31, p. e03133, 2026, doi: 10.1016/j.sciaf.2025.e03133.

[17] C. Wang, B. Sheng, Z. Li, M. Sivan, Z.-Q. Zhang, G.-Q. Li, and S. Q. Xie, "A Lightweight Series Elastic Actuator With Variable Stiffness: Design, Modeling, and Evaluation," *IEEE/ASME Transactions on Mechatronics*, 2023, doi: 10.1109/TMECH.2023.3254813.

[18] J. Chen, Y. Hu, and Z. Gao, "On practical solutions of series elastic actuator control in the context of active disturbance rejection," *Advanced Control for Applications*, vol. 3, no. 2, p. e69, 2021, doi: 10.1002/adc2.69.

[19] S. A. Moafi, E. Abbaszadeh, S. H. Rouhani, S. Mobayen, and F. Najafi, "Empirical reliability enhancement in series elastic actuators using fractional-order finite-time robust control," *Reliability Engineering and System Safety*, vol. 273, p. 112330, 2026, doi: 10.1016/j.ress.2026.112330.

[20] Z. Li, P. Li, Y. Ye, and X. Liu, "A modified active disturbance rejection control method for the compliance control of the flexible joint robots," in *2022 IEEE International Conference on Robotics and Biomimetics (ROBIO)*, 2022, pp. 1813–1818, doi: 10.1109/ROBIO55434.2022.10011734.

[21] P. van Zutven, D. Kostić, and H. Nijmeijer, "Parameter identification of robotic systems with series elastic actuators," *IFAC Proceedings Volumes*, vol. 43, no. 14, pp. 350–355, 2010, doi: 10.3182/20100901-3-IT-2016.00127.

[22] S. Benftima, S. Gharab, A. San-Millan, and V. Feliu-Batlle, "Real Time Mass Estimation of the Payload of a 3-DOF Flexible Links Robot Using an Algebraic Technique Robust to Sensor Offset," *IEEE Robotics and Automation Letters*, vol. 10, no. 2, pp. 1106–1113, 2025, doi: 10.1109/LRA.2024.3513000.

[23] R. Luo, J. Yuan, Y. He, S. Bao, L. Du, and Z. Hu, "Sensorless Payload Estimation of Serial Robots Using an Improved Disturbance Kalman Filter with a Variable-Parameter Noise Model," *Actuators*, vol. 14, no. 12, 2025, doi: 10.3390/act14120568.

[24] S. Zhao and Z. Gao, "An Active Disturbance Rejection Based Approach to Vibration Suppression in Two Inertia Systems," *Asian Journal of Control*, vol. 15, no. 2, pp. 350–362, 2013, doi: 10.1002/asjc.552.

[25] A. S.-M. Rodriguez, J. C. C. Ibañez, and V. F. Battle, "Online Algebraic Identification of the Payload Changes in a Single-Link Flexible Manipulator Moving under Gravity," *IFAC Proceedings Volumes*, vol. 47, no. 3, pp. 8397–8402, 2014, doi: 10.3182/20140824-6-ZA-1003.00397.

BIOGRAPHIES OF AUTHORS

Edwin Villarreal-López received the B.Eng. degree in Design and Electronics Automation Engineering from the Universidad de La Salle, Bogotá, Colombia, in 2004, and the Master's degree in Industrial Automation Engineering from the Universidad Nacional de Colombia, Bogotá, Colombia, in 2008. He is currently pursuing a Ph.D. degree with the Faculty of Engineering at the Universidad Distrital Francisco José de Caldas. He is a Research Associate Professor of the Faculty of Engineering at the Universidad de San Buenaventura, Bogotá, Colombia. His current research interests include fault detection and isolation, active disturbance rejection control, and applications of control theory. He can be contacted at email: evillarreall@libertadores.edu.co.

Horacio Coral-Enriquez received the B.Sc. degree in Engineering in Industrial Automatica from the Universidad del Cauca, Popayán, Colombia, in 2005, and the M.Sc. degree in Automatica from the Universidad del Valle, Cali, Colombia, in 2010. In 2017 he received the Ph.D. degree (Cum laude) from the Universidad Nacional de Colombia. Currently, he is a Research Associate Professor of the Faculty of Engineering at the Universidad de San Buenaventura, Bogotá, Colombia. He is the author of over 40 technical papers in journals and international conference proceedings. His main research areas include active disturbance rejection control, nonlinear control, wind turbine control, and applications of control theory. He can be contacted at email: hcoral@usbbog.edu.co.

Luini L. Hurtado-Cortés received the B.Eng. degree in Mechanical Engineering from the INCCA University, Bogotá, Colombia, in 1995, the Spc. degree in Automation and Industrial Computing from the Universidad Autónoma de Colombia, Bogotá, Colombia, in 2001, and the M.Sc. and Ph.D. degrees in Automation Engineering from the Universidad Nacional de Colombia, Bogotá, Colombia, in 2005 and 2014, respectively. Currently, he is Full Professor of the Faculty of Technology at the Universidad Distrital Francisco José de Caldas, Bogotá, Colombia. His research interests include control systems, supervisory systems, security systems, and robotics applications. He can be contacted at email: llhurtadoc@udistrital.edu.co.